# Modulating alkene reactivity from oxygenation to halogenation via electrochemical O 2 activation by Mn porphyrin

Nikolaos Kostopoulos, Frédéric Banse, Claire Fave, Elodie Anxolabéhère-Mallart

# Modulating alkene reactivity from oxygenation to halogenation *via* electrochemical $O_2$ activation by Mn porphyrin†

Nikolaos Kostopoulos, [a] Frédéric Banse, [b] Claire Fave [a] and Elodie Anxolabéhère-Mallart *[a]

**Oxidation of organic substrates is achieved in nature under mild conditions thanks to metalloenzymes but remains a challenge for chemists. Herein we show by UV-Vis spectroelectrochemistry that when $Mn^{III}$TPPCl is electrochemically reduced to $Mn^{II}$ in $CH_2Cl_2$ under $O_2$, a $Mn^{II}O_2^{\bullet}$ species is generated. Benzoic anhydride reacts with the latter triggering a catalytic current in cyclic voltammetry. Electrolysis on the catalytic wave in the presence of cyclooctene leads to its oxygenation or halogenation depending on the axial ligand present as reported here for the first time.**

Oxidation and halogenation of hydrocarbons are reactions of great importance for the preparation of various organic molecules on an industrial scale. Regarding oxidation reactions (*i.e.* oxygenation and halogenation), hazardous chemical reagents and/or noble metal catalysts are often implemented. Despite its potent oxidizing power and renewable character, $O_2$ is scarcely used in synthetic chemistry under ambient conditions due to its kinetic inertness.[1] By contrast, in Nature, Fe oxygenases achieve highly efficient and selective oxidations by unravelling the $O_2$ potent oxidizing power through its partial and controlled reduction at the Fe active site, leading to O–O bond cleavage to generate the reactive high valent Fe–oxo (FeO).[2] Heme haloperoxidases formally generate their reactive species from the same Fe–oxo (FeO) in presence of $Cl^-$ or $Br^-$ leading to an Cl/BrFeO intermediate able to convert an aliphatic or aromatic C–H bond into a C–Cl/C–Br one.[3]

Fe and Mn porphyrin complexes have been extensively studied as models of the active site of these enzymes[4–6] and have for long been known to be able to oxidize and halogenate organic substrates with oxidizing agents such as $H_2O_2$, *m*-CPBA, PhIO and $OCl^-$. High valent Fe– or Mn–oxo species that are thus produced are responsible of such reactivity.

Since the first example of oxidation of organic molecules by PhIO catalyzed by a Fe porphyrin, reported by Groves[7] there has been numerous publications evidencing oxidation of organic substrates by chemically generated high valent Fe–oxo species.[8] Mn porphyrins are also able to catalyze the halogenation of various substrates with chemical oxidants and more precisely hypochlorite, as recently shown by Groves *et al.*[9,10] However, there are hardly any example of electrochemical oxidation of organic molecules catalyzed by Fe or Mn complexes that occurs by activation of $O_2$.[11]

Among the few examples of electrochemical oxidations by reductive activation of $O_2$ is the pioneering work of Murray[12,13] and the more recent work of Dey,[14] the latter focusing on Fe porphyrins immobilized on SAM. Murray showed that $Mn^{III}$(TPP) can induce epoxidation of cyclooctene under electrocatalytic conditions in good yields in presence of 1-methylimidazole (1-MeIm) and benzoic anhydride. In the present communication we show by means of spectroelectrochemistry that this oxidation process involves a $Mn^{II}O_2^{\bullet}$ adduct as proposed but not proven before. In addition, we show that under the same electrocatalytic conditions but using an excess of chloride instead of 1-MeIm, the oxidation process finally results in the halogenation of cyclooctene.

Fig. 1 displays representative cyclic voltammograms (CVs) of $[Mn^{III}(TPP)Cl]$ (TPP = tetraphenylporphyrinate) under Ar and $O_2$ (air saturated) in a $CH_2Cl_2$ solution. Under Ar atmosphere (Fig. 1, black trace), the $Mn^{III}/Mn^{II}$ wave is quasi reversible with $E_{1/2} = -0.35$ V *vs.* SCE. Under $O_2$ (Fig. 1, red trace), the cathodic current increases and one additional new anodic peak appears at $E_2^a = -0.16$ V *vs.* SCE. The ratio between the two anodic peaks ($E_1^a$ and $E_2^a$) varies with the scan rate and with the temperature as shown in the Fig. S1 and S2 (ESI†). These observations strongly suggest a chemical reaction between $Mn^{II}$ species and $O_2$ and are in accordance with previous works.[12,13,15]

[a] *Université de Paris, Laboratoire d'Electrochimie Moléculaire UMR 7591, CNRS, F-75013 Paris, France. E-mail: elodie.anxolabehere@u-paris.fr*
[b] *Université Paris-Saclay, CNRS, Institut de Chimie Moléculaire et des Matériaux d'Orsay, 91405, Orsay, France*

† Electronic supplementary information (ESI) available. See DOI: 10.1039/d0cc07531k

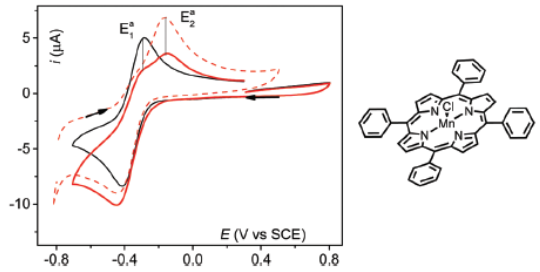


Fig. 1 (left) CVs of 0.5 mM $Mn^{III}$(TPP)Cl in a 0.1 M $TBAPF_6/CH_2Cl_2$ solution on a glassy carbon electrode, at 298 K; under Ar (black trace), under $O_2$ (red trace) and reverse scan under $O_2$ with 15 s delay time at $E_{app} = -0.85$ V (dashed red trace). (right) Schematic structure of $Mn^{III}$(TPP)Cl.

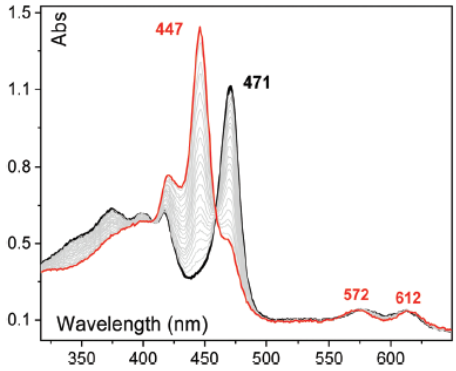


Fig. 2 UV-vis spectrum of 0.1 mM $Mn^{III}$(TPP)Cl, at 298 K, in 0.2 M $TBAPF_6/CH_2Cl_2$ under $O_2$ before applying potential (black trace) and after $E_{app} = -0.45$ V *vs.* SCE, (one spectrum per 20 s, grey traces with final spectrum red trace).

Murray and co-workers[12,13] proposed that $O_2$ binds on the $Mn^{II}$(TPP) generated at the electrode. This new adduct undergoes a one electron reduction, following an ECE mechanism as sketched in Table 1 (mechanism in $CH_2Cl_2$). The one electron reduced species thus formed is claimed to be oxidized at a more positive potential than the $Mn^{II}$(TPP) complex ($E_2^a = -0.16$ V *vs.* $E_1^a = -0.29$ V *vs.* SCE).[12,13,15] This proposition is consistent with the increase of the cathodic current of the $Mn^{III}/Mn^{II}$ when $O_2$ is added in the solution, which excludes, indeed, a simple EC mechanism that would lead to a $Mn^{III}$–superoxo adduct in the diffusion layer.[16] However, to the best of our knowledge, no spectroscopic proof for the formation of the $Mn^{II}$–superoxo ($Mn^{II}O_2^{\bullet}$) or $Mn^{III}$–peroxo ($Mn^{III}OO^-$) intermediate has so far been provided to confirm the above interpretation. To gain further insight into the nature of this electrogenerated species we have performed UV-Vis spectroelectrochemistry.

These experiments were performed either at 298 K or at 258 K using a previously described set-up.[17] Spectra corresponding to $Mn^{III}$ species in $CH_2Cl_2$ were recorded with the characteristic Soret band centered at 471 nm regardless of the atmosphere (Fig. 2, black trace and Fig. S3, ESI†). Under $O_2$ atmosphere upon reduction of a $CH_2Cl_2$ solution of $Mn^{III}$(TPP)Cl at $E_{app} = -0.45$ V *vs.* SCE, a new Soret band appears at 447 nm and simultaneously the $Mn^{III}$ band at 471 fades as shown in Fig. 2 (red trace). The spectral characteristics of the species that accumulates (broad 397 nm, Soret 447 nm, and Q bands at 530, 572 and 612 nm) are identical to those reported for the sample prepared by addition of two equivalents of $KO_2$ in a $Mn^{III}$(TPP) solution in DMSO (broad 398 nm, Soret 446 nm, and Q bands at 530 nm, 572 and 614 nm).[18] A similar UV-Vis spectrum attributed to the formation of a $Mn^{II}$–superoxo species has also been obtained by addition of two equivalents of $KO_2$ in a Mn(TMP) solution (TMP = 5,10,15,20 tetramesitilporphyrinate) in $CH_3CN$.[19] We also propose that, in the present case, the electrochemically generated species is better formulated as a $Mn^{II}O_2^{\bullet}$ ($Mn^{II}$–superoxo) rather than a $Mn^{III}OO^-$ ($Mn^{III}$–peroxo). Indeed, the similarity between the UV-vis spectra obtained under $O_2$ and Ar at $E_{app} = -0.45$ V *vs.* SCE (Fig. S4 and S5, ESI†) suggests that the oxidation state of the metal in these species is the same, *i.e.* +II and not +III (Table 1).

In order to gain further insight into the characteristics of this key intermediate, experiments in DMF, a dissociating solvent, have also been performed. CV of the Mn(TPP)Cl recorded in a DMF solution with 0.1 M $TBAPF_6$ under Ar (Fig. S6, ESI†) shows an important positive shift of the $E_{1/2}$ for the $Mn^{III}/Mn^{II}$ wave compared to those recorded in $CH_2Cl_2$ ($E_{1/2}$ (DMF) = −0.18 V *vs.* $E_{1/2}$ ($CH_2Cl_2$) = −0.35 V).

This behaviour indicates that the $[Mn^{III}(TPP)(DMF)]^+$ form is prominent in this solvent[18] the latter being reduced at more positive potentials. The observed difference in the UV-Vis spectra in DMF and in $CH_2Cl_2$ is also significant and indicative of a change in the coordination sphere (Table 1). Interestingly,

Table 1 Potential values and spectroscopic characteristics of the species generated electrochemically. Proposed mechanisms for the formation of the $Mn^{II}$ superoxo adduct

| | $CH_2Cl_2$ | DMF | | |
|---|---|---|---|---|
| $E_{1/2}(Mn^{III}/Mn^{II})^a$ | −0.347 | −0.178 | Mechanism 1: $CH_2Cl_2$ | Mechanism 2: DMF |
| $Mn^{III b}$ | 471, 575 and 612 | 471, 566 and 601 | | |
| $Mn^{II b}$ | 444, 576 and 616 | 437, 569 and 609 | $\mathbf{E_1}$ $Mn^{III} \overset{e^-}{\rightarrow} Mn^{II}$ $k_1$ | $\mathbf{E_1}$ $Mn^{III} \overset{e^-}{\rightarrow} Mn^{II}$ $k_1'$ |
| $[Mn^{III}/Ar/E_{app} = -0.45]^b$ | 444, 576 and 616 | 437, 569 and 609 | $\mathbf{C}$ $Mn^{II} \overset{O_2}{\rightarrow} Mn^{III}O_2^{\bullet}$ K | $\mathbf{E_2}$ $O_2 \overset{e^-}{\rightarrow} O_2^{-\bullet}$ $k_3$ |
| $[Mn^{III}/O_2/E_{app} = -0.45]^b$ | 447, 570 and 612 | 437, 569 and 609 | $\mathbf{E_2}$ $Mn^{III}O_2^{\bullet} \overset{e^-}{\rightarrow} Mn^{II}O_2^{\bullet}$ $k_2$ | $\mathbf{C}$ $Mn^{II} + O_2^{-\bullet} \rightarrow Mn^{II}O_2^{\bullet}$ K′ |
| $[Mn^{III}/O_2/E_{app} = -1.1]^b$ | — | 447, 570 and 612 | | |

[a] In V *vs.* SCE. [b] In nm.

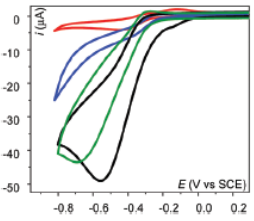


Fig. 3 CVs of 0.5 mM $Mn^{III}$(TPP)Cl in 0.1 M $TBAPF_6/CH_2Cl_2$ solution on a glassy carbon electrode at 298 K with 0.44 M benzoic anhydride under $O_2$ (black trace) and with addition of 20 mM 1-MeIm (blue trace) or with 5 mM TBACl (green trace). For comparison CV under $O_2$ without benzoic anhydride has been added (red trace).

the CV of the $Mn^{III}$(TPP) complex under $O_2$ atmosphere remains unchanged in DMF (see the $Mn^{III}/Mn^{II}$ wave in Fig. S6, ESI†) contrary to what was observed in $CH_2Cl_2$. If more negative potentials are scanned, after the $O_2/O_2^{\bullet-}$ wave (−0.85 V *vs.* SCE), a shoulder at the foot of the $O_2$ reduction wave is observed (Fig. S7A (ESI†), red trace) suggesting a chemical reaction between $Mn^{II}$ and $O_2^{\bullet-}$.[20,21]

Moreover, on the reverse scan, two anodic peaks are observed at −0.78 V and at −0.08 V *vs.* SCE. The former one corresponds to oxidation of free superoxide generated by reduction of excess $O_2$ at the electrode, while the additional peak appearing at a potential close to the one observed in $CH_2Cl_2$ can be ascribed to oxidation of a $Mn^{II}O_2^{\bullet}$ intermediate (Fig. S7B, ESI†). The intensity of this wave suggests a two-electron process as expected for the oxidation of $Mn^{II}O_2^{\bullet}$ to give $Mn^{III}$ and $O_2$. The hypothesis that this key species is formed in DMF following the mechanism 2 (Table 1) is confirmed by spectroelectrochemistry. When a potential of −0.45 V *vs.* SCE is applied in a $Mn^{III}$ solution (Fig. S8A, ESI†), spectra similar to that attributed to the $Mn^{II}$ species are recorded regardless of the atmosphere (Ar or $O_2$).[18] In contrast, when a potential of −1.1 V *vs.* SCE is applied under $O_2$, the spectrum of the $Mn^{II}$(TPP) complex evolves towards a spectroscopic signature identical to the one obtained in $CH_2Cl_2$ and attributed to the $Mn^{II}O_2^{\bullet}$ adduct (Fig. S8B, ESI†). These observations strongly suggest two different mechanisms for the $Mn^{II}$–superoxo formation depending on the solvent. In DMF, the solvent binds the Mn ion (in line with the shift of the Soret and Q bands of the $Mn^{II}$ and of the cathodic peak of the $Mn^{III}$ complex, Table 1) preventing the coordination of the weak donor $O_2$ on the $Mn^{II}$ center, while allowing that of the better donor $O_2^{\bullet-}$ ion (mechanism 2). In the non-coordinating solvent $CH_2Cl_2$, such a competition for the coordination of dioxygen does not occur. As depicted in mechanism 1 (Table 1), it can easily bind to the $Mn^{II}$ center which results in its reduction and formation of the $Mn^{II}O_2^{\bullet}$ intermediate.

Taken into account that the $Mn^{II}O_2^{\bullet}$ intermediate can be generated at a less negative potential in $CH_2Cl_2$ than in DMF (−0.45 *vs.* −1.1 V *vs.* SCE), thus avoiding the concomitant generation of superoxide radicals, we have decided to study the electrocatalytic reactivity of the system for substrate oxidation in $CH_2Cl_2$.

Fig. 3 displays the CV of $Mn^{III}$(TPP)Cl in $CH_2Cl_2$ under $O_2$ in absence (red trace) or in presence of excess benzoic anhydride (880 eq., black trace) (CV under argon, in presence of benzoic anhydride is shown in Fig. S9B, red trace, ESI†). The presence of $O_2$ and benzoic anhydride triggers an increase of the current, indicating a catalytic activity occurring at the onset of the $Mn^{III}/Mn^{II}$ wave. This observation indicates that benzoic anhydride reacts with the $Mn^{II}O_2^{\bullet}$ adduct formed in the diffusion layer. In accordance with the literature, we propose that the catalytic current is due to the O–O bond cleavage[12] *via* the transient generation of an acylperoxo species evolving to a $Mn^{V}O$ species. The $Mn^{V}O$ intermediate can be reduced at the electrode or eventually react with a substrate. In both cases, regeneration of the $Mn^{III}$ species will end the cycle.

Preparative electrolyses under $O_2$ atmosphere at 298 K were first carried out at $E_{app}$ = −0.45 V *vs.* SCE of $Mn^{III}$(TPP)Cl (0.5 mM) in 0.1 M $TBAPF_6/CH_2Cl_2$ solution with excess of benzoic anhydride, and in presence of 1-MeIm (40 equivalents *vs.* Mn) and cyclooctene as substrate (20 equivalents *vs.* Mn). Under these conditions (entry 1, Table 2), cyclooctene oxide was detected with a TON of *ca.* 7.3 after 4 hours electrolysis (see details in ESI†). This result is in accordance with those of Murray *et al.* who used a similar system.[12] It is noteworthy that even though the addition of the 1-MeIm axial base diminished the catalytic current in our case (Fig. 3, blue trace) it is known to significantly improve the yield of the oxidation reactions catalyzed by Mn porphyrins, with $H_2O_2$ as oxidant, by promoting the formation of the $Mn^{V}O$.[22] Indeed that was also the case in the present system (see Table 2, entries 1 and 2). The faradaic yield of the reaction was 81% as calculated from the current *vs.* time plot (Fig. S10A, ESI†).

Then, a preparative electrolysis was performed in presence of 10 eq. of TBACl instead of 1-MeIm (Fig. 3, green trace). In that case, trace amounts of cyclooctene oxide was detected, and chloro-cyclooctene was observed in the chromatogram (Table 2, entry 3 and Fig. S11 for a representative chromatogram, ESI†)

Table 2 Results of preparative scale electrolysis at 298 K under $O_2$. Conditions: 0.5 mM $Mn^{III}$(TPP)Cl, 10 mM alkene and 440 mM benzoic anhydride in 0.1 M $TBAPF_6/CH_2Cl_2$ at $E_{app}$ = −0.45 V *vs.* SCE for 4 h. TON = mole of product/mole of catalyst

| Entry | Substrate | Solvent | 1-MeIm | TBACl | Cyclooctene-oxide | Chlorocyclooctene |
|---|---|---|---|---|---|---|
| 0 | Cyclooctene | $CH_2Cl_2$ | | | Traces | Not detected |
| 1 | Cyclooctene | $CH_2Cl_2$ | 20 mM | — | TON = 7.3 | Not detected |
| 2 | Cyclooctene | $CH_2Cl_2$ | 20 mM | 5 mM | TON = 7.1 | Not detected |
| 3 | Cyclooctene | $CH_2Cl_2$ | — | 5 mM | Traces | TON = 4.8 |
| 4 | Cyclooctene | $CH_2Cl_2$ | — | 40 mM | Traces | TON = 1.6 |
| 5 | Cyclooctene | DMF | — | 40 mM | Not detected | Not detected |

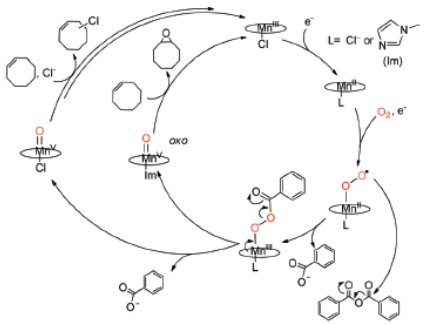

**Scheme 1** Activation of $O_2$ catalyzed by Mn(TPP)Cl in $CH_2Cl_2$, in the presence of benzoic anhydride, and 1-MeIm or $Cl^-$ leading to oxygenation or chlorination of cyclooctene, respectively.

with TON = 7.1. When the same solution was subjected to a second preparative electrolysis after addition of 1-MeIm, cyclooctene was produced but no more chlorinated compound (Fig. S11, blue trace, ESI†). The faradaic yield calculated from Fig. S10B (ESI†) was 53%. An increase of TBACl concentration did not induce any increase of the yield but rather a slight decrease (Table 2, entry 4). This observation can be ascribed to a coordination of $Cl^-$ to the Mn center in competition with $O_2$, in accordance with the decreased catalytic current observed in the presence of $Cl^-$ (compare black and green traces in Fig. 3). Along the same line, the nature of the solvent plays an important role as one could anticipate from the cyclic voltammetry study (*vide supra*). Replacing $CH_2Cl_2$ by DMF (Table 2, entry 5) leads to a total inhibition of the reactivity, as the result of the coordination of DMF.

Scheme 1 summarizes a proposed mechanism for the observed reactivity which emphasizes the role of the exogenous ligand, *i.e.* 1-methylimidazole or chloride. When neither of the two is in solution, almost no reaction takes place (Table 2, entry 0). If 1-MeIm is added (with or without chloride in solution), the oxygenation reaction is favored with formation of epoxide.[9] When chloride is added (without 1-MeIm), only chlorination reaction takes place. To rationalize these observations, we propose two different mechanistic pathways depending on the nature of the 6$^{th}$ ligand (Scheme 1). As shown above, a $Mn^{II}O_2^{\bullet}$ is formed at the electrode polarized at −0.45 V which further reacts with benzoic anhydride to generate a $Mn^{III}$–acylperoxo intermediate. The presence of the *trans* 1-MeIm ligand promotes the heterolytic cleavage to give a $Mn^{V}O$ species responsible for the oxygenation of cyclooctene. In the presence of excess $Cl^-$ instead of 1-MeIm, the selectivity of the reaction is completely changed towards halogenation of the substrate. While a systematic study of this reaction has not yet been performed, it is tempting to propose that the $Mn^{V}O$ active intermediate would preferentially react with the anion rather the olefin to yield a chlorinating agent (Cl radicals and $Mn^{IV}O$ or $Mn^{III}$–OCl).

In conclusion, in this communication we bring insights into the mechanism of $O_2$ reductive activation by a Mn porphyrin, and explore new routes of reactivity under electrocatalytic conditions. We provide the first spectroscopic evidences that a $Mn^{II}O_2^{\bullet}$ adduct is formed in the $Mn^{III}/Mn^{II}$ wave ($E_{1/2}$ = −0.35 V *vs.* SCE) in presence of $O_2$ in $CH_2Cl_2$. In DMF the formation of the same intermediate occurs *via* the interaction of $Mn^{II}$ ion with electrochemically generated $O_2^{\bullet-}$ at a more negative potential ($E_{1/2}(O_2/O_2^{\bullet-})$ = −0.75 V *vs.* SCE). We then also show that oxidative transformation of cyclooctene is possible under electrocatalytic conditions at the $Mn^{III}/Mn^{II}$ wave in $CH_2Cl_2$ in presence of benzoic anhydride: when an excess of $Cl^-$ is added the reaction is directed towards chlorination of the substrate, whereas cyclooctene-oxide is selectively formed when 1-MeIm is used. We have now in hands a simple way to direct the reaction pathway from oxygenation to halogenation by simple swapping of the exogenous ligand.

NK acknowledges the French government for his PhD fellowship. NK thanks Martin Kientz for his help during the acquisition and the analysis of the GC/MS data. Support from GDR MAPYRO and GIS FrenchBic is acknowledged.

## Conflicts of interest

There are no conflicts to declare.

## Notes and references

1 F. Cavani and J. H. Teles, *ChemSusChem*, 2009, **2**, 508–534.
2 I. G. Denisov, T. M. Makris, S. G. Sligar and I. Schlichting, *Chem. Rev.*, 2005, **105**, 2253–2278.
3 J. Latham, E. Brandenburger, S. A. Shepherd, B. R. K. Menon and J. Micklefield, *Chem. Rev.*, 2018, **118**, 232–269.
4 X. Huang and J. T. Groves, *Chem. Rev.*, 2018, **118**, 2491–2553.
5 R. A. Baglia, J. P. T. Zaragoza and D. P. Goldberg, *Chem. Rev.*, 2017, **117**, 13320–13352.
6 S. Sahu and D. P. Goldberg, *J. Am. Chem. Soc.*, 2016, **138**, 11410–11428.
7 J. T. Groves, T. E. Nemo and R. S. Myers, *J. Am. Chem. Soc.*, 1979, **101**, 1032–1033.
8 W. Nam, *Acc. Chem. Res.*, 2007, **40**, 522–531.
9 W. Liu and J. T. Groves, *J. Am. Chem. Soc.*, 2010, **132**, 12847–12849.
10 G. Li, A. K. Dilger, P. T. Cheng, W. R. Ewing and J. T. Groves, *Angew. Chem., Int. Ed.*, 2018, **57**, 1251–1255.
11 E. Anxolabéhère-Mallart and F. Banse, *Curr. Opin. Electrochem.*, 2019, **15**, 118–124.
12 S. E. Creager, S. A. Raybuck and R. W. Murray, *J. Am. Chem. Soc.*, 1986, **108**, 4225–4227.
13 S. E. Creager and R. W. Murray, *Inorg. Chem.*, 1987, **26**, 2612–2618.
14 M. Mukherjee and A. Dey, *ACS Cent. Sci.*, 2019, **5**, 671–682.
15 G. Passard, D. K. Dogutan, M. Qiu, C. Costentin and D. G. Nocera, *ACS Catal.*, 2018, **8**, 8671–8679.
16 J.-M. Savéant, *Chem. Rev.*, 2008, **108**, 2348–2378.
17 N. Kostopoulos, C. Achaibou, J. M. Noel, F. Kanoufi, M. Robert, C. Fave and E. Anxolabéhère-Mallart, *Inorg. Chem.*, 2020, **59**, 11577–11583.
18 J. S. Valentine and A. E. Quinn, *Inorg. Chem.*, 1976, **15**, 1997–1999.
19 J. T. Groves, Y. Watanabe and T. J. McMurry, *J. Am. Chem. Soc.*, 1983, **105**, 4489–4490.
20 R. Oliveira, W. Zouari, C. Herrero, F. Banse, B. Schöllhorn, C. Fave and E. Anxolabéhère-Mallart, *Inorg. Chem.*, 2016, **55**, 12204–12210.
21 N. Ségaud, E. Anxolabéhère-Mallart, K. Sénéchal-David, L. Acosta-Rueda, M. Robert and F. Banse, *Chem. Sci.*, 2015, **6**, 639–647.
22 P. Battioni, J. P. Renaud, J. F. Bartoli, M. Reina-Artiles, M. Fort and D. Mansuy, *J. Am. Chem. Soc.*, 1988, **110**, 8462–8470.